Title	Control of optical rogue waves in supercontinuum generation with a minute continuous wave
Author(s)	Li, Q; Zhang, C; Cheung, KKY; Qiu, Y; Tsia, KK; Wong, KKY; Li, F; Lau, APT; Wai, PKA
Citation	The 2011 Conference on Lasers and Electro-Optics (CLEO 2011), Baltimore, MD., 1-6 May 2011. In Conference on Lasers and Electro-Optics Proceedings, 2011.
Issued Date	2011
URL	http://hdl.handle.net/10722/135879
Rights	Conference on Lasers and Electro-Optics Proceedings. Copyright © IEEE.

Control of Optical Rogue Waves in Supercontinuum Generation with a Minute Continuous Wave

Qian Li[1], Chi Zhang[2], Kim K. Y. Cheung[2], Yi Qiu[2], Kevin K. Tsia[2], Kenneth K. Y. Wong[2], Feng Li[1], Alan Pak Tao Lau[1], and P. K. A. Wai[1,*]

[1]*Photonics Research Centre, Department of Electronic and Information Engineering, The Hong Kong Polytechnic University, Hung Hom, Hong Kong*

[2]*Department of Electrical and Electronic Engineering, The University of Hong Kong, Pokfulam Road, Hong Kong*

[*]*enwai@polyu.edu.hk*

Abstract: We numerically demonstrate that optical rogue wave in supercontinuum generated with picosecond pulse can be controlled by a minute continuous wave.

OCIS codes: (060.4370) Nonlinear optics, fibers; (320.6629) Supercontinuum generation

1. Introduction

Supercontinuum (SC) generation in optical fibers has been the subject of extensive research in the past ten years. SC coherence is one of the key factors in accessing potential applications. Although it is well known that SC coherence can be greatly improved in SC generation using femtosecond pulses, such ultrashort pulses are sensitive to perturbation and hence are not practical in many applications. Subsequent work has considered SC properties when pump pulse varies from picosecond to continuous wave regime. An important nonlinear process in the SC generated with long pulses is the modulation instability (MI) which adds sidebands to narrow band input radiation. While soliton fission is the dominating effect in the SC generation using femtosecond pulses, MI is particularly important for long input pulses. Since MI growth starts spontaneously from noise, the resulting SC can become incoherent away from the pump wavelength [1]. Solli et al. have shown that the SC generated with picosecond pulses contains a small number of statistically-rare "rogue" events [2]. After that, there has been a great interest in the study of optical rogue waves, which is a noise-sensitive nonlinear process exhibiting extreme value statistics with long-tailed probability distributions. Here we theoretically demonstrate the rogue wave instability can be controlled by simply applying a weak continuous wave (CW) signal. Compared to prior works which show the active control of SC can be realized by using a pulse-seeding [1] or a THz intensity modulation of the input pulse [3], our CW-triggering technique requires only wavelength tuning which makes it a much simpler approach to achieve active control of SC.

2. Numerical Model

Our simulation is based on the generalized nonlinear Schrödinger equation [4]

$$\frac{\partial A}{\partial z}+i\frac{\beta_2}{2}\frac{\partial^2 A}{\partial t^2}-\frac{\beta_3}{6}\frac{\partial^3 A}{\partial t^3}=i\gamma\left(1+i\tau_{shock}\frac{\partial}{\partial t}\right)A(z,t)\int_{-\infty}^{+\infty}R(t')\left|A(z,t-t')\right|^2 dt', \tag{1}$$

where $A(z,t)$ is the field envelope, $\tau_{shock}=1/\omega_0$ where ω_0 is the center frequency, β_2, β_3 and γ are the second and third order dispersion and nonlinear coefficients. The Raman response function $R(t)=(1-f_R)\delta(t)+f_R h_R(t)$. We use $f_R=0.18$ and h_R determined from the experimental fused silica Raman cross-section [4]. Input pulse noise is included in the frequency domain through a (random phase) one photon per mode spectral density on each spectral discretization bin [5]. We simulate a 5.8-ps FWHM chirp-free Gaussian pulse with peak power of 60 W, and center wavelength at 1554.5 nm propagating in a commercially available 50-m highly nonlinear dispersive fiber (HNL-DSF) with zero dispersion wavelength (ZDW) at 1554 nm, nonlinear coefficient γ = 14/W/km, second order and third order dispersion coefficients at the 1554 nm pump wavelength are β_2 = -0.0224 ps^2/km and β_3 = 0.0576 ps^3/km respectively.

3. Results

Fig. 1 shows the results without CW seeding. The dashed curve in Fig. 1(a) is the numerical spectrum obtained by averaging 200 simulations corresponding to 200 different realizations of initial input noise. The most red-shifted soliton is centered at around 1843 nm. For a small number of events in the ensemble, we find the SC spectrum extends significantly further towards longer wavelength beyond 1965 nm as illustrated by the solid curve in Fig. 1(a). The dashed curve and solid curve in Fig. 1(b) represent the input pulse, and the temporal profile after passing the

output spectrum (solid curve in Fig. 1(a)) through a red-pass filter with the cut wavelength at 1700 nm. The tallest pulse in Fig. 1(b) is 865 W. Fig. 1(c) shows the wavelength dependence of the first order coherence $|g_{12}^{1}(\lambda)|$. We calculate $|g_{12}^{1}(\lambda)|$ using the method described in [4]. $|g_{12}^{1}(\lambda)|$ lies in the interval [0,1], and a value of 1 denotes perfect coherence. Only a narrow band close to the pump wavelength has relatively good coherence. Fig. 1(d) shows the peak power histogram for around 1000 events (pulses) after a red-pass filter with the cut wavelength at 1700 nm. Here and in the following, the around 1000 events correspond to those in the 200 simulations with different realization of initial input noise, and only the pulses with peak power larger than the pump, and pulse-to-pulse separation larger than the average width of the pulses are counted. Clearly, the histogram for heights is sharply peaked but has a very long tail. Fig. 2 shows the results when a weak CW is added in the input. All the other parameters are same as Fig. 1. The weak CW is adjusted to be at 1497 nm, and its intensity is only 1/10000 of the pump. The dashed curve in Fig. 2(a) is the numerical spectrum obtained by averaging 200 simulations corresponding to 200 different realizations of initial input noise. The solid curve in Fig. 2(a) is one realization of the output spectrum, which contains the rogue event. The dashed curve and solid curve in Fig. 2(b) represent the input pulse, and the temporal profile after passing the output spectrum (solid curve in Fig. 2(a)) through a red-pass filter with the cut wavelength at 1700 nm. The tallest pulse in Fig. 2(b) is 1250 W. Fig. 2(c) shows the wavelength dependence of first order coherence. Clearly, the coherence has been greatly improved compared to Fig. 1(c). Besides a much wider band around the pump wavelength, two sidebands also appear. Fig. 2(d) shows the peak power histogram for around 1000 events (pulses) after a red-pass filter with the cut wavelength at 1700 nm. The distribution has changed to a normal distribution. Comparing the average output spectrum, the one in Fig. 1(a) varies from 1248 nm to 2076 nm at -10 dBm and the total energy after the red-pass filter at 1700 nm is 366 W, while the one in Fig. 2(a) varies from 1239 nm to 2106 nm at -10 dBm and the total energy after the red-pass filter at 1700 nm is 422 W.

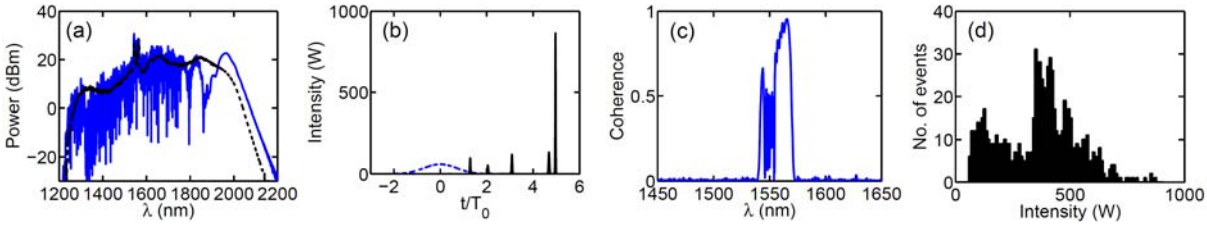

Fig. 1. Results without CW seeding. (a) Dashed curve and solid curve represent the average output spectrum and output spectrum which contains rogue event; (b) dashed curve and solid curve represent the input pulse, and the temporal profile after passing the output spectrum (solid curve in Fig. 1(a)) through a red-pass filter with the cut wavelength at 1700 nm; (c) degree of first-order coherence; (d) histogram of the peak power distribution using 9 W bins.

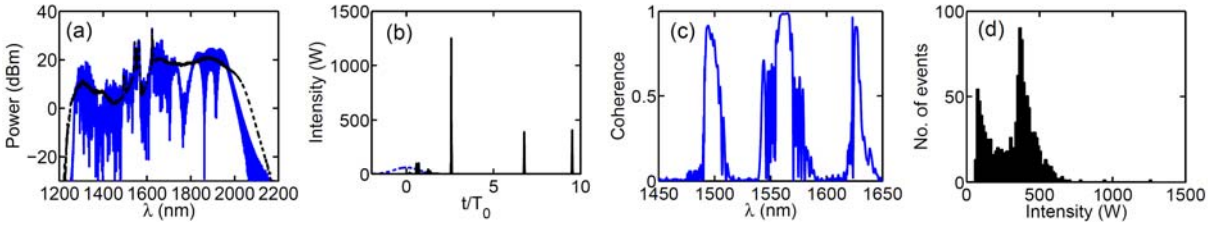

Fig. 2. Results with CW seeding. (a) Dashed curve and solid curve represent the average output spectrum and output spectrum which contains rogue event; (b) dashed curve and solid curve represent the input pulse, and the temporal profile after passing the output spectrum (solid curve in Fig. 2(a)) through a red-pass filter with the cut wavelength at 1700 nm; (c) degree of first-order coherence; (d) histogram of the peak power distribution using 15 W bins.

4. Conclusion

We theoretically demonstrate the rogue wave instability can be controlled by simply applying a weak CW signal.

5. References

[1] D. R. Solli, C. Ropers, P. Koonath and B. Jalali, "Active Control Rogue Waves for Stimulated Supercontinuum Generation," Phys. Rev. Lett., **101**, 233902 (2008).

[2] D. R. Solli, C. Ropers, P. Koonath and B. Jalali, "Optical rouge waves," Nature **450**, 1054 (2007).

[3] G. Gently, J. Dudley and B. Eggleton, "Modulation control and spectral shaping of optical fiber supercontinuum generation in the picosecond regime," Appl. Phys. B: Lasers Opt., **94**, 187 (2009).

[4] J. M. Dudley, G. Genty and S. Coen, "Supercontinuum generation in photonic crystal fiber," Rev. Mod. Phys., **78**, 1135 (2006).

[5] J. M. Dudley, G. Genty and B. J. Eggleton, "Harnessing and control of optical rogue waves in supercontinuum generation," Opt. Express **16**, 3644 -3651 (2008).